Journal of Biomedical Optics

SPIEDigitalLibrary.org/jbo

Elucidation of the mechanisms of optical clearing in collagen tissue with multiphoton imaging

Vladimir Hovhannisyan
Po-Sheng Hu
Shean-Jen Chen
Chang-Seok Kim
Chen-Yuan Dong

SPIE

Elucidation of the mechanisms of optical clearing in collagen tissue with multiphoton imaging

Vladimir Hovhannisyan,[a] Po-Sheng Hu,[a] Shean-Jen Chen,[b] Chang-Seok Kim,[c] and Chen-Yuan Dong[a,c,d]
[a]National Taiwan University, Department of Physics, Taipei 106, Taiwan
[b]National Cheng-Kung University, Department of Engineering Science, Tainan 701, Taiwan
[c]Pusan National University, Department of Cogno-Mechanotronics Engineering, Busan, Republic of Korea
[d]National Taiwan University, Center for Quantum Science and Engineering, Taipei 106, Taiwan

Abstract. Optical clearing (OC) is a promising method to overcome limitations in biomedical depth-resolved optical studies. Mechanisms of OC in purified bovine Achilles tendon, chicken skin, and chicken tendon were studied using time-lapsed, three-dimensional second harmonic generation (SHG) and two-photon fluorescence microscopic imaging. Quantified nonlinear optical measurements allowed temporal separation of two processes in collagen OC with glycerol. The first one is a fast process of tissue dehydration accompanied with collagen shrinkage and the second relatively slow process is glycerol penetration into the interfibrillar space of collagen alongside with CF swelling. The use of 50% glycerol induced less-expressed OC via partial substitution of water molecules with glycerol molecules. We also found that phosphate-buffered saline- and glycerol-treatments were reversible, and fiber morphology and SHG signal intensity were recovered after the removal of immersion agents. It was shown that tissue OC was a dynamic process and elucidation of its physical mechanisms may help choose optimal diagnostic, treatment, and modification regimes for collagen-based as well as other types of biomaterials. [DOI: 10.1117/1.JBO.18.4.046004]

Keywords: second harmonic generation; multiphoton microscopy; collagen; tendon; optical clearing.

Paper 12818R received Dec. 21, 2012; revised manuscript received Feb. 12, 2013; accepted for publication Mar. 12, 2013; published online Apr. 2, 2013; corrected Apr. 4, 2013.

1 Introduction

Reduction of light scattering in biological tissues can essentially enhance the efficacy of laser-based applications in biomedicine. Optical clearing (OC) is an effective method to overcome the limitations of multiphoton microscopy caused by turbidity of biological materials.[1,2] The application of an optical clearing agent (OCA) to blood,[3] skin,[4–7] brain,[8] muscle,[9,10] bone,[11] and other turbid biological tissues[12–16] temporarily reduces optical scattering and increases light transparency. As a result, in most cases, OC improves signal contrast and sensitivity and spatial resolution of optical diagnostic techniques such as fluorescence spectroscopy,[2] Raman spectroscopy,[11] optical diffusion tomography,[4,5] optical coherence tomography,[3,4,15] confocal imaging,[8] and nonlinear microscopy.[1,2,9,10] Specifically, through the use of a novel OCA, *in vivo* human skin OC was demonstrated for the first time.[5] Another remarkable scientific milestone attributing to OC was the 3D visualization of neural wiring networks of *Drosophila* at cellular resolution without tissue sectioning, which allowed construct of a virtual fly brain.[17] Furthermore, an interesting application of optically cleared collagen-based tissue was suggested recently.[18] In this case, transparency of 57% at 550 nm through air-dehydration of a rabbit dermis was achieved and it was shown that such OC can be preserved by chemically induced cross-linking. The induced optical transparency was preserved during a 4-week autogenic transplantation of the tissue into the rabbit corneal stromal pocket.

In addition to the development of safe and more effective OCAs for biomedical applications, the elucidation of OC mechanisms may lead to improved development of OC strategies. In particular, with the increasing applications of lasers in surgery, diagnostics, and therapeutics, it is important to understand how OCAs interact with biological tissues, cells, and molecules such as collagen, a major component of the intracellular matrix. Currently, explanations of the OC mechanisms of collagen fiber (CF) by the use of glycerol and other hyperosmotic agents remain inconsistent. Previously, two mechanisms for reducing light scattering in biological materials by the use of OCAs have been suggested. The first is tissue dehydration caused by the introduction of the hyperosmotic agent, resulting in tight and uniform packing of optical scattering components.[19,20] The second mechanism is matching of refractive indices of the clearing media and the extracellular matrix.[20,21] However, in one study, through the use of second harmonic generation (SHG) imaging and polarization light microscopy on tendon, native skin, and engineered skin specimens, a new mechanism for tissue OC was suggested.[22] In this particular case, glycerol was used as the OCA, and it was found that backward SHG (BSHG) signal vanished and the CF banding pattern, which was revealed under polarization light microscopy, disappeared. Therefore, CF dissociation was proposed as a molecular mechanism for glycerol-mediated OC. Subsequent application of phosphate-buffered saline (PBS) led to the recovery of SHG intensity, and it was suggested that re-association of high-order collagen fibrous structure occurred when glycerol was removed.[22] Molecular basis of OC in collagenous tissue induced by chemical agents were investigated using a combination of molecular dynamics simulations and optical spectroscopy.[23]

Address all correspondence to: Chen-Yuan Dong, National Taiwan University, Department of Physics, Taipei 106, Taiwan. Tel: +8862-3366-5155; Fax: +8862-3366-5244; E-mail: cydong@phys.ntu.edu.tw

The conclusion that hyperosmotic OCAs caused adverse effects on collagen-containing tissues was supported by another study,[9] in which a decrease in the forward SHG (FSHG) intensity from mouse tail tendon treated with a medium containing 50% glycerol was demonstrated, and it was concluded that collagen OC was not enhanced. However, no significant effects of glycerol on collagen fibrillar pattern as well as on the supramolecular organization of acto-myosin complexes were observed.[9,10] Similarly, transmission electron microscopy revealed that collagen fibril organization was not destroyed by glycerol, and glycerol treatment resulted in more densely packed collagen arrays.[19,24] Furthermore, optical coherence tomography (OCT) and photographic images of tendon and skin treated with glycerol and air-drying indicated that OC mechanism in collagenous tissues was mainly tissue dehydration.[19] Yu et al., developed a partial least squares regression model based on reflectance spectra in the range of 1100 to 1700 nm to quantitatively investigate the dehydration of skin, and concluded that dehydration was the main mechanism of skin OC for 1,2-propanediol, 1,4-butanediol, or PEG200 during the 60 min topical treatment, whereas for PEG400, glycerol, or D-sorbitol, other mechanisms that further enhance OC besides the dehydration should exist.[25]

The role of backscattering in SHG tissue imaging was discussed in a previously reported study,[12] and it was shown that BSHG image obtained for thick turbid tissue, such as tendon, was a result of a significant contribution of the FSHG signal that was backscattered toward the focusing objective in addition to the direct BSHG signal. Also, authors clearly demonstrated that any variation in the linear scattering properties of tissues can strongly affect BSHG image formation.

In this work, we attempted to perform a comprehensive quantitative study to elucidate physical mechanisms of glycerol-induced OC in collagen-based tissues through multiphoton imaging. We investigated the dynamics of collagen OC on samples that have undergone air-drying, 100% glycerol, and 50% glycerol solution treatment. By the acquisition and analysis of FSHG, BSHG, and two-photon fluorescence (TPF) imaging, the effects of OC on bovine Achilles tendon (BAT), chicken tendon and skin are studied.

2 Materials and Methods

Multiphoton imaging was achieved using a laser scanning microscope system (LSM 510 META, Zeiss, Jena, Germany) coupled to a femtosecond (fs) titanium:sapphire laser operating in the wavelength of 780 nm and repetition rate of 80 MHz (Tsunami, Spectra-Physics, Mountain View, CA). The nominal value of the laser pulse-width was around 120 fs and the *in situ* average power was between 5 to 50 mW. Two Zeiss, Plan-Neofluar air objectives ($20\times$/NA 0.5, working distance (WD) = 1.3 mm and $10\times$/NA 0.3, WD = 3 mm) were used for imaging. The detection bandwidths of the BSHG and TPF signals were 380 to 400 nm and 435 to 700 nm, respectively.

The collagen specimens included dry, type I collagen from BAT (27662, Fluka, Switzerland), and native CFs from chicken leg tendon (CLT), and chicken skin. The excised tissue specimens were briefly washed in PBS (Invitrogen, Auckland, New Zealand) and immediately mounted on the microscope well chamber. As an OC agent, we used either absolute glycerol (Fisher Scientific, Hampton, New Hampshire) or PBS solution containing 50% glycerol. The images were analyzed with ImageJ (National Institutes of Health, http://rsb.info.nih.gov/ij/).

For the comparison of BSHG and FSHG detection modes and quantification of the OC effect, we placed aluminum foil behind the upper section of CF, which allows the collection of a considerable portion of FSHG signal through reflection. Concurrently, the bottom most section of CF was covered up by a layer of fluorescent plastic sheet that emits TPF signal for the dynamic tracking of CF transparency during OC; and the middle section was used for BSHG imaging. The schematic arrangement of CF, an aluminum foil, and a fluorescent plastic sheet is presented in Fig. 1.

3 Results

3.1 *Optical Clearing of the Purified Collagen Fibers*

For imaging and quantification of the OC effect, we performed experiments on purified CF from BAT first. Purified BAT is used in an effort to obtain repeatable and statistically reliable results, and exclude the influence of other proteins and compounds that may participate in OC of biological tissues as discussed previously.[9] Also, in these experiments, we took into account the displacement of the image plane during the drying and immersion of samples in media with different optical indices, and axially discriminated scan of samples was performed in such a way that the scan depth was larger than the entire sample thickness, and the pixel dwell time was small enough to provide 30 s for three-dimensional imaging of the sample. Next, the axial stack was averaged using ImageJ software to acquire the final multiphoton image. In this manner, we acquired time-lapsed multiphoton images of CF from BAT during the OC process with PBS and 100% glycerol. The representative multiphoton images are shown in Fig. 2(a)–2(g), where pseudo color red represents SHG signal from CF, and green represents TPF from fluorescent plastic plate, which is partially shielded by bottom-most section of CF. The SHG signal from the upper section of CF above dashed line in Fig. 2(a)–2(g) is more than three times stronger than that from the rest of CF and can be considered as FSHG signal because the aluminum foil placed behind the CF reflects the forwardly directed SHG signal back to the focusing objective for collection and registration. The SHG image below dash line represents SHG signal backscattered within the specimen, which can be considered as BSHG signal. Quantitative data

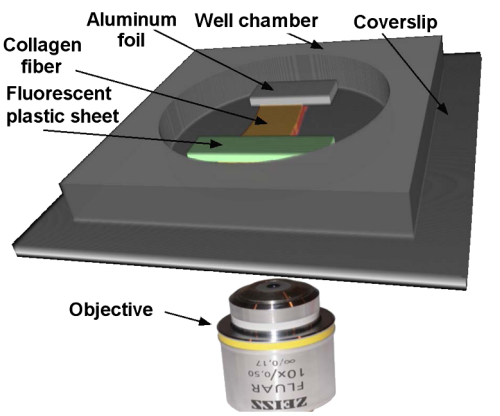

Fig. 1 Schematic arrangement of the microscope well chamber.

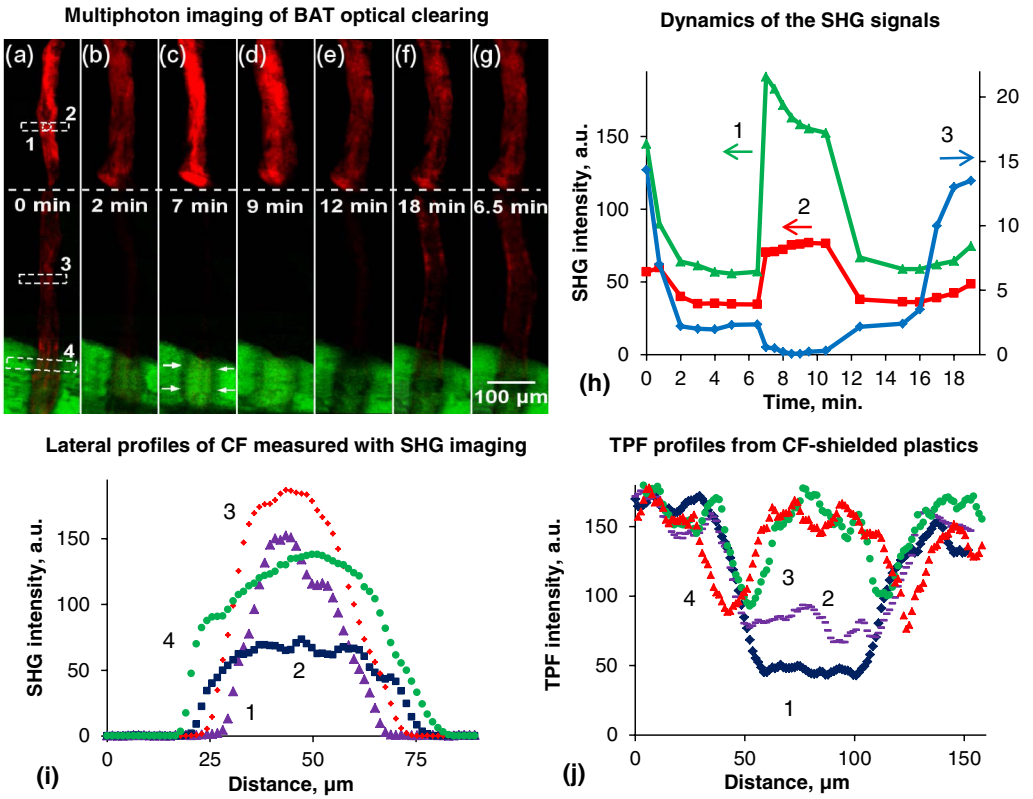

Fig. 2 Time-lapsed multiphoton imaging of the optical clearing process in CF from BAT using PBS and 100% glycerol. Multiphoton images of (a) dry CF; (b) CF immersed in PBS for 2 min; (c) PBS-treated CF after immersion in glycerol for 0.5 min, and (d) for 2.5 min; (e) CF after glycerol elution and subsequent treatment with PBS for 2 min; (f) wet CF after treatment with glycerol for 6 min and washed by PBS; and (g) wet CF after PBS elution and prior to being treated with glycerol. (h) Temporal dependence of SHG intensity from (1) ROI 1 (local FSHG), (2) ROI 2 (total FSHG), and (3) ROI 3 (total BSHG) shown in panel (a). (i) Lateral profiles of FSHG intensity of (1) dry CF [see panel (a)], (2) CF immersed in PBS for 2 min (b), (3) CF immersed in glycerol for 0.5 min (c), and (4) for 2.5 min (d) from ROI 2 at different stages of the OC process. (j) Lateral profiles of averaged TPF intensity of CF-shielded plastics recorded along ROI 4 in the panels (a)–(g) of (1) dry CF (panel a), (2) CF immersed in PBS for 2 min (b), (3) CF immersed in glycerol for 0.5 min (c), and (4) for 2.5 min (d). 20 × /NA 0.5 objective was used throughout the experiments.

characterizing the dynamics of nonlinear signals and lateral profiles of CF are presented in Fig. 2(h)–2(j).

First, the temporal dependences of SHG signal from different ROI shown in Fig. 2(a) are presented in Fig. 2(h). Herein, Series 1 is the plot of local FSHG intensity from a circular ROI 1 inside the CF, Series 2 is the plot of total FSHG intensity collected within the rectangular ROI 2, which covered a segment of the fiber along the lateral direction, and Series 3 is total BSHG intensity from ROI 3. Series 1 and 2 clearly delineate nonproportionality of local FSHG and the total FSHG, which can be attributed to the changes in geometrical sizes of CF and collagen density during the process of OC.

The effects of CF shrinkage and swelling during OC were studied by measuring FSHG intensity profile across CF [Fig. 2(a), ROI 2 and 3] and are illustrated in Fig. 2(i). Finally, the variation in CF transparency under the application of PBS and glycerol is shown in Fig. 2(j), where the intensity profiles of TPF of CF-shielded plastics were measured within ROI 4 shown in Fig. 2(a).

When dry CF was immersed in PBS, local FSHG, total FSHG and BSHG intensities decreased rapidly (in less than 2 min) by a factor of 2.5, 1.6, and 7.1, respectively [Fig. 2(i), Series 1, 2, and 3]. At the same time, swelling of the fiber and the increase in the lateral dimensions by a factor 1.75 were observed [Fig. 2(i), Series 1 and 2]. Because the used BAT consisted of fibers insoluble in water, and disassociation of the CF was not observed during PBS immersion, the decay of BSHG intensity may be attributed to the decrease in FSHG scattering due to the partial refractive index matching as water (with optical index $n = 1.33$) penetrated into the CF and replaced the air, resulting in a better matching of refractive index to that of dry collagen ($n = 1.53$). The same mechanism of partial OC was responsible for approximately 1.7-fold increase in the TPF from the fluorescent plastics sheets at the site shielded with CF [Fig. 2(j), Series 1 and 2]. Reduction of FSHG intensity may be associated with the decrease of collagen fibril density within the focal volume, which was caused by penetration of water molecules into the CFs.

More complex processes occurred when the samples were treated with glycerol. After the removal of PBS residues and addition of 100% glycerol, CF shrank rapidly by a factor of about 1.5 during the first 30 sec of immersion [Fig. 2(c) and 2(i), Series 2 and 3]. In parallel with CF shrinkage, there was an increase in local and total FSHG intensities by factors of 3.4 and 2.1, respectively, as well as 5.8-fold decrease in BSHG intensity [Fig. 2(h), Series 1, 2, and 3, time-points 6.5 and 7 min]. The shrunken state of CF did not preserve well in glycerol as the lateral sizes of the fiber increased by approximately 50% during the next 2 to 3 min. Correspondingly, due to the expansion in lateral dimension and the reduction of the collagen density the local FSHG intensity at a selected ROI 1 dropped by 30% and stabilized eventually, whereas some

increase in total FSHG intensity [Fig. 2(h), Series 1 and 2] was recorded. The decrease in BSHG and the increase in total FSHG intensities can be associated with the decrease in scattering and glycerol-induced OC upon CF. The TPF imaging further confirmed the effects of the glycerol-induced OC in that the CF immersed in glycerol became increasingly transparent during the first phase (CF shrinking) [Fig. 2(c) and 2(j), Series 3], and the second phase (CF swelling) did not alter the optical transparency of the CF since the level of the TPF intensities remained during the process of OC [Fig. 2(d) and 2(j), Series 4]. Thus, both SHG and TPF imaging indicated that the penetration of glycerol molecules into CF and the subsequent swelling of CF preserved the effect of OC rendered by glycerol-induced dehydration. Presence of opacity was still observed along CF edges [Fig. 2(c), 2(d), and 2(j), Series 3 and 4], where weaker TPF may be caused by strong scattering of the excitation light with very small incident angle at the CF edges.

An intuitive follow-up step was to verify whether the glycerol-induced processes in CF were reversible. After the removal of residual glycerol and addition of PBS, CF-induced SHG pattern and intensity level almost reverted to the state observed in PBS-immersed CF prior to glycerol treatment [see Fig. 2(b) and 2(e), 2(h), 6 and 15 min time points]. Moreover, the complete reversibility of glycerol impact upon the CF became rather obvious if we compared the glycerol-treated CF image obtained in air with the CF image taken prior to glycerol application [Fig. 2(f) and 2(g)], where BSHG signal was observed as well. Panel (g) is shown next to panel (f) for a better comparison, which shows that qualitatively, temporal glycerol treatment does not change CF morphological structure and SHG signal. Interesting result relevant to OC mechanism obtained using time-lapsed nonlinear imaging of purified CF samples was the distinction of glycerol-induced shrinkage (dehydration) observed in first 30 sec of glycerol application as well as subsequent swelling and glycerol penetration into the interfiber space of CF. Furthermore, volume and shape of CF as well as BSHG and FSHG signals responded differently during these processes. Nonetheless, we found that these changes were reversible and tissue morphology revealed by SHG imaging was restored within few minutes after glycerol removal, which supported the statement that CF did not undergo dissociation under glycerol treatment.

3.2 *Optical Clearing of Chicken Collagenous Tissues*

Similar approach was applied to estimate the effect of air-drying on a tendon sample resected from fresh chicken leg in that one third of posterior side of the CLT sample was covered up by fluorescent plastics for retrieving TPF signal [bottom segment

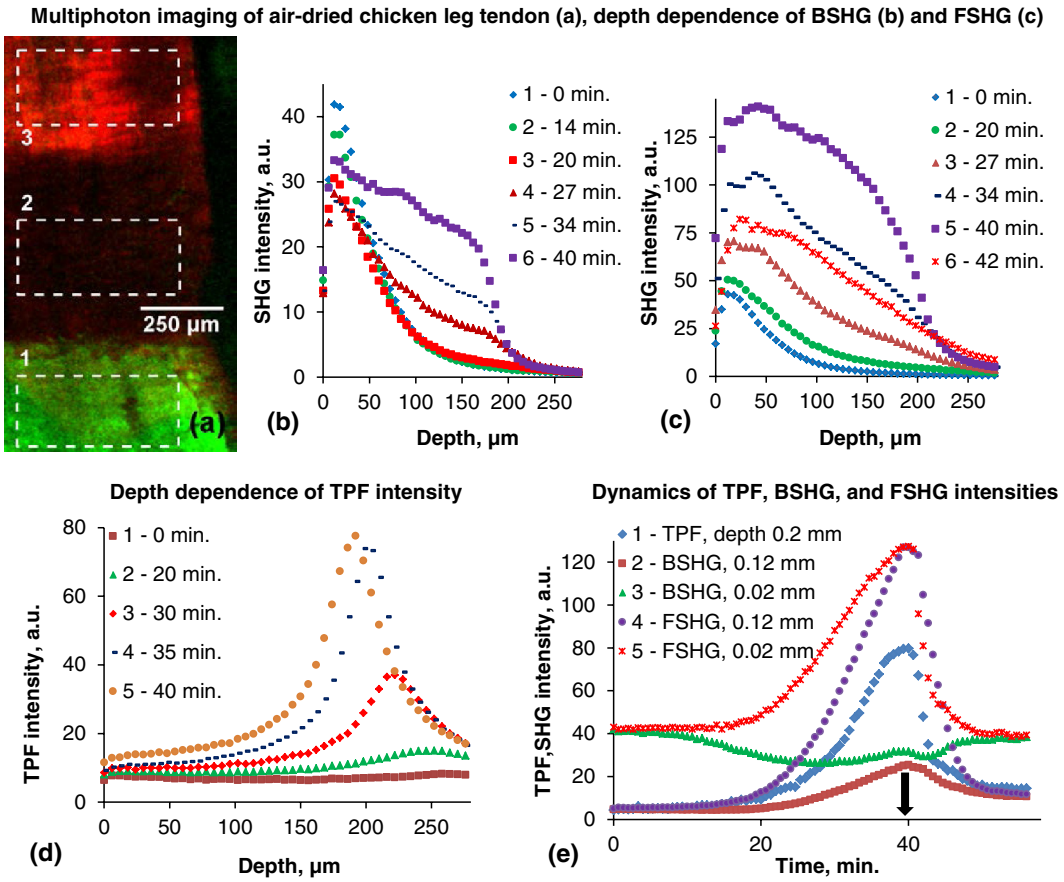

Fig. 3 (a) Multiphoton image of fresh chicken leg tendon, acquired at the depth of 220 μm with a 10 × NA 0.3 objective. Pseudocolors green and red represent TPF signal from fluorescent plastic sheet placed behind the CF, and SHG signal from CF, respectively. (b) Axially discriminated SHG intensity profiles of the air-dried CLT acquired from ROI 2 (BSHG) and (c) ROI 3 (FSHG) shown in panel (a). (d) TPF intensity profiles acquired from ROI 1. (e) Temporal dependence of TPF, BSHG, and FSHG signals during air-dried and subsequent rehydration by the application of PBS at the time-point indicated by the arrow.

of the multiphoton image shown in Fig. 3(a)], and upper segment of the sample was covered up using aluminum foil with the middle portion left uncovered. At last, we performed time-lapsed, axially discriminated scan of the sample during the dehydration.

Axial SHG intensity profiles from the CLT sample are shown in Fig. 3(b) and 3(c). The original sample was about 0.35 mm in thickness, and at the time of 0 min it was air-dried by the removal of PBS solution. Following dehydration, the sample was rehydrated by adding PBS to the well at the 40 min time point. Experimental series in Fig. 3(b) and 3(c) are related to ROIs 2 and 3 in Fig. 3(a) correspondingly. These graphs show that imaging depth, defined as a depth when SHG intensity drops two times relative to maximal intensity, increases with the period of the drying time and reaches the far edge of the sample [Fig. 3(b), Series 6 and Fig. 3(c), Series 5]. It can also be seen that maximal intensity of BSHG signal from ROI 2 in Fig. 3(a) drops by a factor of 1.3 [Fig. 3(b), Series 1 and 5], whereas FSHG signal emanated within ROI 3 upon reflection of an aluminium cover increases monotonically by a factor of 3.2 [Fig. 3(c)]. As for comparison, axial profile of FSHG signal taken at 2 min after wetting is shown [Fig. 3(c), Series 6].

Furthermore, time-lapsed axial profiles of TPF intensity extracted from the fluorescent plastic sheet overlying the tendon sample are shown in Fig. 3(d). During air-drying, the localization of maximal intensity in these profiles shifts from 258 μm (Series 1) to 192 μm (Series 5), and the intensity maximum increased by a factor of 45. The shifting of maximal intensity and decrease in the optical thickness of the specimen are caused by the shrinkage in specimen thickness and the increase in sample refractive index during air-drying.[19]

Dynamics of TPF, BSHG, and FSHG intensities were acquired from ROIs 1, 2, and 3, during the periods of air-drying (0 to 40 min) and rehydration (40 to 56 min) [Fig. 3(e)]. In the initial stage of the sample dehydration, BSHG intensity was reduced (Series 3) due to the decrease of backscattering of the FSHG signal; however, the scattering of tendon did not vanish, which was possibly attributed to air content within CF. Further, drying and OC processes contributed more effective focusing, and as a result, an increase in both FSHG and BSHG intensities was observed (Series 1–5).

We also studied the processes of OC in chicken skin through the use of 100% and 50% glycerol, and depth and temporal dependence of SHG intensity are shown in Fig. 4. Particularly, the results showed that the depth of FSHG registration increased from 50 μm to greater than 500 μm [Fig. 4(a), Series 1 and 4], and BSHG emanated from shallow depths [Fig. 4(c), Series 1] decreased to background level in 10 to 12 min after glycerol application, suggesting an occurrence of significant reduction in scattering. One can use the ratio of maximal FSHG intensity at the end of clearing period to BSHG or FSHG intensity at the beginning of an OC process as an indicator of the commencement of the process. In this manner, the ratios were determined [Figs. 3(c), 4(a), and 4(c)] to be 3.1, 4.75, and 1.7 for air-dried, 100% and 50% glycerol treatments, respectively, which verified that the application of 100% glycerol, as an OC agent, was more effective than 50% glycerol or air-drying.

Furthermore, we quantitatively investigated the effects of shrinkage and swell in CLT along lateral and longitudinal directions of fiber, and the magnitudes of changes during the OC were monitored using marks engraved by femtosecond laser microlithography (Fig. 5).[26]

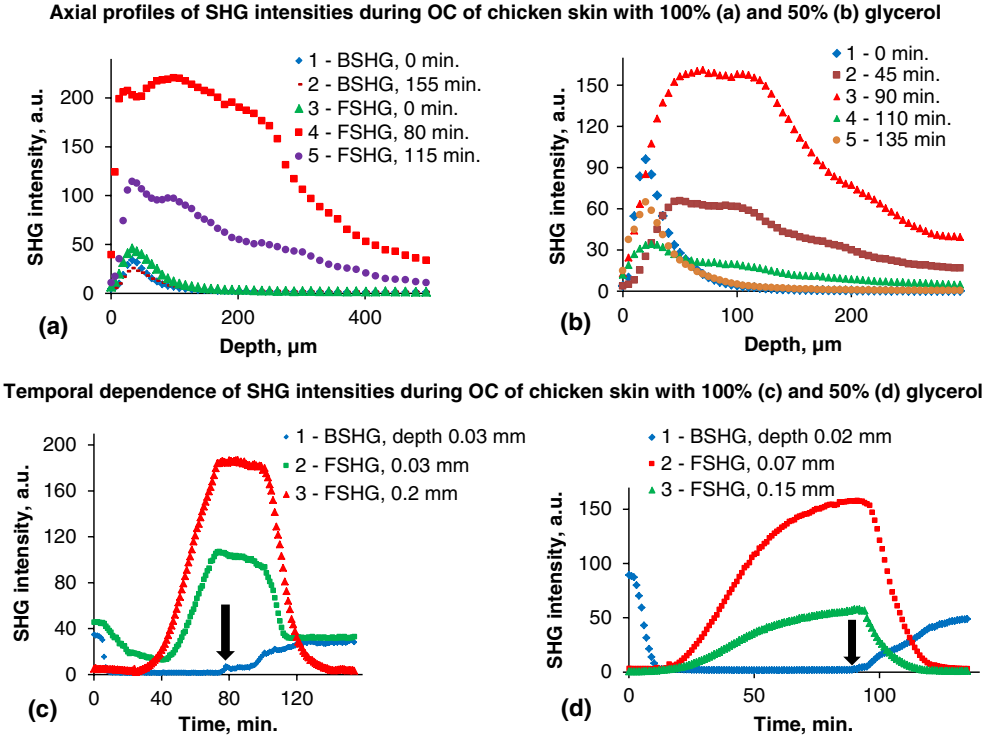

Fig. 4 The profiles of axially (a) and (b) and temporally (c) and (d) dependent BSHG and FSHG intensities during OC of chicken skin with 100% (a) and (c) and 50% (b) and (d) glycerol and the following rehydration, in which glycerol was subsequently replaced with PBS at time points of 75 min and 95 min [indicated by the arrows in (c) and (d)].

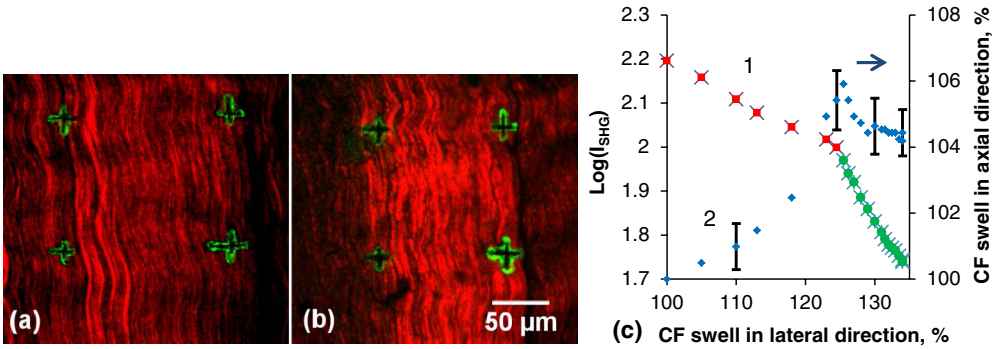

Fig. 5 Multiphoton imaging of (a) a wet tendon sample from CLT where 4 marks (+) were laser-engraved; (b) the sample after drying for 40 min. The change in distance between engraved marks indicates shrinkage of tendon fibers during the air-drying process. Pseudocolors green and red represent TPF from laser-induced photoproducts and SHG from collagen, respectively. Fs laser with average power of 50 mW, centered wavelength at 780 nm, and 20 × /NA 0.5 objective lens were used for laser lithography and multiphoton imaging. (c) The dependence of FSHG intensity (Series 1) and axial elongation (Series 2) upon lateral dimension expansion in percentage during the treatment of chicken tendon with PBS.

We measured the distances between two pairs of crosses along axial and lateral directions of the fiber based on both SHG and TPF images [Fig. 5(a) and 5(b)] as well as averaged FSHG intensity recorded during the tendon hydration with the application of PBS. The dependencies of FSHG intensity as well as the averaged relative elongation on averaged relative enlargement in lateral dimension are shown in Fig. 5(c). It is clearly seen that trends of both FSHG intensity (Series 1) and CF elongation (Series 2) change significantly as the lateral dimension is swollen by 125%, which indicates that two sequential processes in tendon fiber hydration have been observed. We conjecture that first process is the penetration of water into interfibrillar space, resulting in the decrease of total number of CF in imaging area and the corresponding reduction in SHG intensity. It is supposed that during the subsequent hydration and lateral dimension enlargement, water molecules also penetrate into intrafibrillar space, which results in the decrease of collagen fibril density. During this process the decaying trend of SHG intensity becomes more drastic due to the quadratic dependence of SHG on collagen molecules density.[27]

Finally, it was observed that glycerol-induced OC of tendon resulted in bright, narrowly directed SHG signal, which can be recorded by consumer photo or video camera (Fig. 6). The laser-scanning process upon samples, with a mean laser power of 50 mW, wavelength in the range of 830 to 900 nm, and 10 × /NA 0.3 focusing objective, can be seen with naked eyes using 400 to 450 nm bandpass filter.

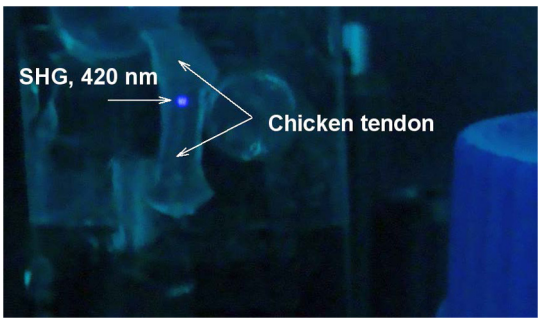

Fig. 6 Forwardly directed SHG signal from CLT (312 mm) treated with glycerol for 20 min was captured by a consumer photo-camera as indicated by the arrow pointing at a dark blue spot. Laser radiation with 840 nm wavelength and 100 mW output power was delivered to a spot of 0.5 mm in diameter.

4 Discussion

Native collagen-based biomaterials are widely used as optimal biocompatible substitutes in studies related to tissue engineering and regenerative medicine.[28] Posterior to OC and stabilization by chemically induced cross-linking procedures collagen may be used in ocular treatments as well. Although previously implemented air-drying OC method provided partial transparency,[18] application of hyperosmotic agents such as glycerol and proper OC regime were the ones that can essentially improve optical properties of the collagen tissue. Nonetheless, the mechanism of OC was not completely understood, and side effects were observed in many research studies, including *in vivo* experiments.[5,9,24]

In this paper, we reproduced and analyzed experiments on collagen OC using glycerol and air-immersion. Similar to previous results,[22] we found SHG signal of glycerol-treated collagen disappeared in backward detection geometry. Additionally, it was shown that BSHG signal was reduced by a factor of 7.1 upon hydration of dry CF with PBS, whereas simultaneously recorded FSHG signal dropped by a factor of 1.6. In case of OC using glycerol, the depth of FSHG registration increased from 50 μm to greater than 500 μm along with incremental loss of image resolution for deeper layers. Furthermore, using TPF imaging, an increase from 40% up to close to 100% in transparency of collagen sample with the thickness of 70 μm as well as 45-fold hike of TPF signal at the depth of 250 μm were verified. Finally, it was shown that glycerol-induced OC was a reversible process, and CF morphology and intensity of both BSHG and FSHG signals reverted to the preclearing levels after glycerol removal and subsequent CF immersion in PBS. The SHG signal, emanated from purified CF of BAT with length of 0.9 mm and diameter of 70 μm recovered in less than 6 min, which indicated that the dissociation of collagen fibrils and subsequent re-association were unlikely as the portion of the dissociated molecules would have been removed together with glycerol.

The decaying trend of BSHG served as an indicator of collagen fibril disassembly in the processes such as thermal denaturation,[29] laser destruction,[22] and carcinogenesis.[30] However, in the case of glycerol-induced OC, such decrease in BSHG intensity is a consequence of the reduction in light scattering within samples and can be used for the measurement of OC efficiency. For collagen structure, since the coherence length of BSHG (40 nm) is much smaller than that of FSHG (7 μm), the primary

BSHG signal generated alongside with FSHG is 2 to 4 orders of magnitude lower than that of FSHG.[27] Nonetheless, in highly scattered biological tissues such as tendon, skin, bone, and cartilage, the enhanced OC leads to an increase of FSHG and a decrease in BSHG intensities (Figs. 2–4, 6).

Collagen shrinkage was the key effect in OC described in previous studies.[10,18,22–24] Specifically, OCT measurement showed that air and 100% glycerol immersion resulted in 1.3-fold shrinkage in lateral dimension of CF.[18] In addition, the authors observed 1.35-fold weight loss and concluded that dehydration was the main mechanism of glycerol OC. Shrinkage of dermis thickness was also observed *in vivo* experiments implemented with 100% glycerol.[24] Our experiments showed concomitant shrinkage with incremental SHG signal intensity during both processes of CF air-drying and glycerol immersion (Figs. 2, and 3). Oppositely, swelling effect of CF was pronounced during PBS-immersion process upon dry CF, or CF with prolonged (>30 sec) immersion in 100% glycerol (Figs. 2, 4, 5). The swelling process of CF was also observed during the treatment with 50% glycerol,[9] which was further proven by the thickening of the dermis under *in vivo* treatments of 20% and 40% glycerol.[24] Furthermore, transmission electron microscopy demonstrated that 30% glycerol in phosphate buffer induced a largely recoverable expansion of the interfibrillar space, and yet, the characteristic axial period of 67 nm in collagen fibrils was maintained.[31]

In addition, our experiments showed that local FSHG signal dropped simultaneously with CF swelling, and, more importantly, glycerol-induced swelling did not impair the sample transparency (Figs. 2 and 3).

Time-lapsed multiphoton microscopy allowed temporal separation of two processes in high concentration glycerol-induced OC. First, there was a fast process that resulted in sample dehydration and shrinkage. The second process was slower penetration of glycerol molecules into the CFs and a simultaneous decrease in collagen density (swelling). The first process was accompanied with increase and second one with decrease in SHG intensities. When glycerol was diluted with water, a partial replacement of water molecules with glycerol molecules occurred, thus, the proportion of glycerol content in the solution and the duration of OC determined the dominant effects on CF shrinkage or swelling. Quantitatively, OC can be described by the simple, heuristic particle-interaction model,[32,33] which predicts that the reduced scattering coefficient (μ_s cm^{-1}) for a densely distributed scattering particles is related to the reduced scattering cross-section for a single particle (σ_s cm^{-1}) through $\mu_s = \Phi(1-\Phi)\sigma_s/V$, where Φ is the volume fraction of scattering particles and V is the volume of a single scattering particle. With the decrease of water content, the volumetric fraction of collagen will increase ($\Phi \to 1$), and thereby, μ_s approaches to 0. Note that OC through the optical index matching can also be described by this formula considering that $\sigma_s \sim \Delta n^2$, where Δn is the difference between optical indices of OCA and the clearing material. Therefore, in case of the first mechanism of OC (dehydration) optical index of OCA plays secondary role, whereas for the second mechanism (the replacement of water molecules with OCA molecules) optical indices matching of OCA and collagen and/or other tissues components is crucial.

Finally, we captured SHG signal from chicken tendon after the OC utilizing glycerol by a consumer photo camera during femtosecond laser illumination, and were convinced that forwardly directed SHG signal can be seen by naked eyes when the sample was scanned by fs laser beam with 830-900 nm wavelengths. These effects were not observed in any tissue with non-OC treated, opaque collagen, and open new perspectives in SHG imaging/photography of biological tissues and live organs.

5 Conclusions

In summary, based on multimodal, quantitative nonlinear microscopic studies, we showed that tissue OC was a dynamic process and specified OC mechanisms of CF. First one is a fast process of tissue dehydration accompanied with collagen shrinkage and the second, relatively slow process is glycerol penetration into the interfibrillar space of collagen alongside with CF swelling. The available data suggested that the glycerol treatment of collagen was not destructive, and yet, an effective tool for OC of collagen-based materials. Elucidation of the physical mechanisms of OC can be used for optimization of optical diagnostics and laser therapy upon tissues as well as for the effective modification of collagen-based materials.

Acknowledgments

This study was financially supported by the National Science Council, Taiwan (NSC 101-2112-M-002-003-MY3), National Taiwan University (NTU-102R7804), Center for Quantum Science and Engineering (CQSE-102R891401), National Health Research Institutes (NHRI-EX101-10041EI), and the World Class University Program at Pusan National University.

References

1. O. Nadiarnykh and P. J. Campagnola, "Retention of polarization signatures in SHG microscopy of scattering tissues through optical clearing," *Opt. Express* **17**(7), 5794–5806 (2009).
2. S. Vesuna, R. Torres, and M. J. Levene, "Multiphoton fluorescence, second harmonic generation, and fluorescence lifetime imaging of whole cleared mouse organs," *J. Biomed. Opt.* **16**(10), 106009 (2011).
3. V. V. Tuchin, X. Xu, and R. K. Wang, "Dynamic optical coherence tomography in studies of optical clearing, sedimentation, and aggregation of immersed blood," *Appl. Opt.* **41**(1), 258–271 (2002).
4. G. Vargas et al., "Use of an agent to reduce scattering in skin," *Lasers Surg. Med.* **24**(2), 133–141 (1999).
5. M. Khan et al., "Optical clearing of *in vivo* human skin: implications for light based diagnostic imaging and therapeutics," *Lasers Surg. Med.* **34**(2), 83–85 (2004).
6. M. H. Khan et al., "Can topically applied optical clearing agents increase the epidermal damage threshold and enhance therapeutic efficacy?," *Lasers Surg. Med.* **35**(2), 93–95 (2004).
7. R. Cicchi et al., "Contrast and depth enhancement in two-photon microscopy of human skin *ex vivo* by use of optical clearing agents," *Opt. Express* **13**(7), 2337–2344 (2005).
8. A. S. Chiang et al., "Three-dimensional reconstruction of brain-wide wiring networks in Drosophila at single-cell resolution," *Curr. Biol.* **21**(1), 1–11 (2011).
9. S. Plotnikov et al., "Optical clearing for improved contrast in second harmonic generation imaging of skeletal muscle," *Biophys. J.* **90**(1), 328–339 (2006).
10. R. Lacomb et al., "Quantitative second harmonic generation imaging and modeling of the optical clearing mechanism in striated muscle and tendon," *J. Biomed. Opt.* **13**(2), 021109 (2008).
11. M. V. Schulmerich et al., "Optical clearing in transcutaneous Raman spectroscopy of murine cortical bone tissue," *J. Biomed. Opt.* **13**(2), 021108 (2008).
12. F. Légaré, C. Pfeffer, and B. R. Olsen, "The role of backscattering in SHG tissue imaging," *Biophys. J.* **93**(4), 1312–1320 (2007).
13. X. Q. Xu, R. K. Wang, and J. B. Elder, "Optical clearing effect on gastric tissues immersed with biocompatible chemical agents investigated

by near infrared reflectance spectroscopy," *J. Phys. D Appl. Phys.* **36**(14), 1707–1713 (2003).
14. V. V. Tuchin, R. K. Wang, and A. T. Yeh, "Optical clearing of tissues and cells," *J. Biomed. Opt.* **13**(2), 021101 (2008).
15. I. V. Larina et al., "Enhanced OCT imaging of embryonic tissue with optical clearing," *Laser Phys. Lett.* **5**(6), 476–479 (2008).
16. E. A. Genina, A. N. Bashkatov, and V. V. Tuchin, "Tissue optical immersion clearing," *Expert Rev. Med. Devic.* **7**(6), 825–842 (2010).
17. H. H. Lin et al., "A map of olfactory representation in the Drosophila mushroom body," *Cell* **128**(6), 1205–1217 (2007).
18. Y. Tanaka et al., "Irreversible optical clearing of rabbit dermis for autogenic corneal stroma transplantation," *Biomaterials* **32**(28), 6764–6772 (2011).
19. C. G. Rylander et al., "Dehydration mechanism of optical clearing in tissue," *J. Biomed. Opt.* **11**(4), 041117 (2006).
20. V. V. Tuchin et al., "Light propagation in tissues with controlled optical properties," *J. Biomed. Opt.* **2**(4), 401–417 (1997).
21. V. V. Tuchin, *Optical Clearing of Tissues and Blood*, SPIE, Bellingham, WA (2005).
22. A. T. Yeh et al., "Reversible dissociation of collagen in tissues," *J. Invest. Dermatol.* **121**(6), 1332–1335 (2003).
23. J. M. Hirshburg et al., "Molecular basis for optical clearing of collagenous tissues," *J. Biomed. Opt.* **15**(5), 055002 (2010).
24. X. Wen et al., "*In vivo* skin optical clearing by glycerol solutions: mechanism," *J. Biophotonics* **3**(1–2), 44–52 (2010).
25. T. Yu et al., "Quantitative analysis of dehydration in porcine skin for assessing mechanism of optical clearing," *J. Biomed. Opt.* **16**(9), 095002 (2011).
26. V. Hovhannisyan et al., "Dynamics of femtosecond laser photo-modification of collagen fibers," *Opt. Express* **16**(11), 7958–7968 (2008).
27. R. M. Williams, W. R. Zipfel, and W. W. Webb, "Interpreting second harmonic generation images of collagen I fibrils," *Biophys. J.* **88**(2), 1377–1386 (2005).
28. R. Parenteau-Bareil, R. Gauvin, and F. Berthod, "Collagen-based biomaterials for tissue engineering applications," *Materials* **3**(3), 1863–1887 (2010).
29. V. A. Hovhannisyan, P. J. Su, and C. Y. Dong, "Quantifying thermodynamics of collagen thermal denaturation by second harmonic generation imaging," *Appl. Phys. Lett.* **94**(23), 233902 (2009).
30. S. M. Zhuo et al., "Quantitatively linking collagen alteration and epithelial tumor progression by second harmonic generation microscopy," *Appl. Phys. Lett.* **96**(21), 213704 (2010).
31. L. Leonardi et al., "Light microscopy, electron microscopy, and x-ray diffraction analysis of glycerinated collagen fibers," *J. Ultrastruct. Res.* **85**(2), 228–237 (1983).
32. V. Twersky, "On scattering of waves by random distributions. II. Two-space scatterer formalism," *J. Math. Phys.* **3**(4), 724–734 (1962).
33. H. Liu et al., "Dependence of tissue optical properties on solute-induced changes in refractive index and osmolarity," *J. Biomed. Opt.* **1**(2), 200–211 (1996).